Turbulence Reduces Magnetic Diffusivity in a Liquid Sodium Experiment

Simon Cabanes, Nathanaël Schaeffer, and Henri-Claude Nataf*
Université Grenoble Alpes, ISTerre, F-38000 Grenoble, France and CNRS, ISTerre, F-38000 Grenoble, France
(Received 6 August 2014; published 28 October 2014)

The contribution of small scale turbulent fluctuations to the induction of a mean magnetic field is investigated in our liquid sodium spherical Couette experiment with an imposed magnetic field. An inversion technique is applied to a large number of measurements at Rm ≈ 100 to obtain radial profiles of the α and β effects and maps of the mean flow. It appears that the small scale turbulent fluctuations can be modeled as a strong contribution to the magnetic diffusivity that is negative in the interior region and positive close to the outer shell. Direct numerical simulations of our experiment support these results. The lowering of the effective magnetic diffusivity by small scale fluctuations implies that turbulence can actually help to achieve self-generation of large scale magnetic fields.

DOI: 10.1103/PhysRevLett.113.184501 PACS numbers: 47.27.-i, 47.32.Ef, 47.65.-d, 52.30.Cv

The Earth, the Sun, and many other astrophysical bodies produce their own magnetic field by dynamo action, where the induction of a magnetic field by fluid motion overcomes the Joule dissipation. In all astrophysical bodies, the conduction fluid undergoes turbulent motion, which can also significantly affect the induction of a large-scale magnetic field by either enhancing it or weakening it. It is therefore of primary interest to quantify the role of these fluctuations in the dynamo problem.

The induction equation for the mean magnetic field $\langle \mathbf{B} \rangle$ reads

$$\frac{\partial \langle \mathbf{B} \rangle}{\partial t} = \nabla \times (\langle \mathbf{U} \rangle \times \langle \mathbf{B} \rangle + \mathcal{E}) + \eta \Delta \langle \mathbf{B} \rangle, \qquad (1)$$

where $\langle U \rangle$ is the mean velocity field, $\eta = (\mu_0 \sigma)^{-1}$ is the magnetic diffusivity (involving the magnetic permeability μ_0 and the conductivity of the fluid σ), and $\mathcal{E} = \langle \tilde{\mathbf{u}} \times \tilde{\mathbf{b}} \rangle$ is the mean electromotive force (emf) due to small scale fluctuating magnetic $\tilde{\mathbf{b}}$ and velocity $\tilde{\mathbf{u}}$ fields. The relative strength between the inductive and dissipative effects is given by the magnetic Reynolds number $\mathrm{Rm} = UL/\eta$ (U and L are the characteristic velocity and the characteristic length scale). When there is a scale separation between the turbulent fluctuations and the mean flow, we can follow the mean-field theory and expand the emf in terms of mean magnetic quantities: $\mathcal{E} = \alpha \langle \mathbf{B} \rangle + \beta \nabla \times \langle \mathbf{B} \rangle$. For homogeneous isotropic turbulence, α and β are scalar quantities. α is related to the flow helicity and results in an electrical current aligned with the mean magnetic field, whereas β can be interpreted as a turbulent diffusivity effectively increasing ($\beta > 0$) or decreasing ($\beta < 0$) electrical currents. The effective magnetic diffusivity $\eta_{\mathrm{eff}} = \eta + \beta$ can have tremendous effects on energy dissipation and on dynamo action by reducing or increasing the effective magnetic Reynolds number $\mathrm{Rm}_{\mathrm{eff}} = UL/\eta_{\mathrm{eff}}$.

However, direct determination of these small-scale contributions remains a challenging issue for experimental studies and numerical simulations.

First generation dynamo experiments were designed to show that turbulent flows with strong geometrically imposed helicity could self-generate their own magnetic fields. Since the success of Riga [1] and Karlsruhe [2] dynamos, several other liquid metal experiments have sought to overcome the effects of magnetohydrodynamic turbulence in less constrained, more geophysically relevant, flow geometries. Unfortunately, dynamo action remains elusive, and the effective contribution of small-scale motions to large-scale magnetic fields remains poorly understood, though the small-scale motions seems to work against dynamo action [3,4].

In the Perm torus-shaped liquid sodium experiment, the effective magnetic diffusivity was inferred from phase shift measurements of an alternating magnetic signal, indicating turbulent increases in magnetic diffusivity of up to ≈30% [4]. The Madison experiment, a sphere containing two counter-rotating helical vortices, found that an externally applied magnetic field was weakened by about 20% at Rm = 130, which they interpreted as a negative global α effect [3]. The installation of an equatorial baffle was found to reduce the amplitude of the largest-scale turbulent eddies and hence the α effect [5]. In the same setup, Rahbarnia *et al.* [6] measured the local emf directly, finding contributions from both α and β, but with a dominant β effect. They reported an increase in magnetic diffusivity of about 30%. The von Kármán Sodium experiment, a cylinder containing another two-vortex liquid sodium flow, reported a magnetic diffusivity increase of about 100% [7].

We analyze data from the Derviche Tourneur Sodium (DTS) experiment, a magnetized spherical Couette flow experiment sketched in Fig. 1. Forty liters of liquid sodium are enclosed between an inner sphere (radius $r_i = 74$ mm) and a concentric outer stainless steel shell (inner radius

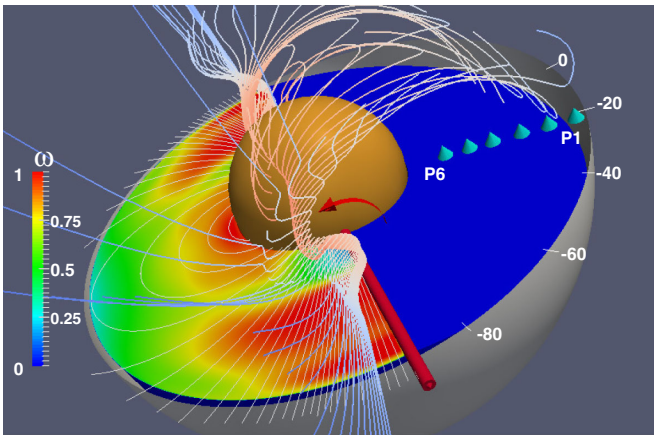

FIG. 1 (color online). Sketch of the DTS experiment with its liquid sodium contained between an outer stainless steel shell (gray, with latitude labels in degrees) and an inner copper sphere (orange), which spins as indicated by the red arrow around the vertical rotation axis (here tilted for clarity). Left half of the sphere: the field lines of the dipolar magnetic field imposed by the central magnet are drawn on top of the contour map of the fluid angular velocity ω (normalized by that of the inner sphere) inverted from data measured for $\mathrm{Rm} = 94$. Right half of the sphere: field lines of the total reconstructed magnetic field. The field lines are strongly distorted by the flow (ω effect). The blue cones mark the radial positions of the six magnetometers $P1$ ($r = \text{radius}/r_o = 0.99$) to $P6$ ($r = 0.50$), which measure the azimuthal magnetic field. They can be placed at four different latitudes (here $-20°$).

$r_o = 210$ mm). The inner sphere can rotate around the vertical axis at rates up to $f = 30$ Hz, yielding a maximal value of 94 for the magnetic Reynolds number defined as $\mathrm{Rm} = 2\pi f r_o^2/\eta$. The inner sphere consists of a copper shell containing a strong permanent magnet, which produces a, mostly dipolar, magnetic field pointing upwards along the rotation axis. The intensity of the magnetic field decreases from $B_i \simeq 180$ mT at the equator of the inner sphere to $B_o \simeq 7.1$ mT at the equator of the outer shell. More details are given in Ref. [8].

In a recent study [9], we developed a new strategy to determine the mean velocity and induced magnetic fields. Following earlier works [8,10], we collect ultrasound Doppler velocity profiles, electric potential measurements, global torque, and measurements of the induced magnetic field inside the sodium layer to reconstruct meridional maps of the mean flow and magnetic field at a given Rm, taking into account the link established by the induction equation. But we further constrain these fields by analyzing the response of the fluid shell to a time-periodic magnetic field, as in Frick *et al.* [4]. In our case, the time-periodic signal simply results from the rotation of our central magnet, whose small deviations from axisymmetry produce a field varying at the rotation frequency and its harmonics. We have expanded the complete magnetic potential of the magnet in spherical harmonics up to degree 11 and order 6, which we then use to compute the solution of the time-dependent induction equation. The predictions for a given mean velocity field are compared to actual magnetic measurements inside the sodium shell at four latitudes and at six radii, as depicted in Fig. 1. We construct a nonlinear inversion scheme of the induction equation to retrieve the mean axisymmetric (and equatorially symmetric) toroidal and poloidal velocity fields that minimize the difference between the predictions and all measurements at a given rotation rate f of the inner sphere. Cabanes *et al.* [9] discuss in detail the solutions and fits for $\mathrm{Rm} = 28$.

In the present study, we extend the analysis to the largest available $\mathrm{Rm} = 47$, 72, and 94 (see Table I for details). Figure 1 displays a meridional map of the angular velocity inverted for $\mathrm{Rm} = 94$, and the field lines of the predicted magnetic field. They confirm that, near the equator of the inner sphere where the magnetic field is strong, the angular velocity stays nearly constant along magnetic field lines (Ferraro law [11]). That region displays superrotation, while the flow becomes more geostrophic further away from the inner sphere.

However, the mean velocity field alone does not fully account for the measured mean magnetic field. Figueroa *et al.* [12] point out that velocity fluctuations invade the interior of the shell in the DTS experiment as the rotation rate f increases, and that magnetic fluctuations always get larger towards the inner sphere because of the strong imposed magnetic field there. We therefore extend our previous approach [9] to take into account the contribution of turbulent fluctuations to the mean magnetic field. Following earlier attempts [3,4,6], we choose to invert for α and β, but since we expect that fluctuations will strongly depend upon the intensity of the mean magnetic field, we allow them to vary with radius. Note that time-varying magnetic signals are particularly sensitive to the effective magnetic diffusivity, hence to β [4,13].

We thus simultaneously invert for the mean axisymmetric toroidal velocity field $U_T(r,\theta)$ and for radial profiles $\alpha(r)$ and $\beta(r)$. U_T is decomposed in spherical harmonics up

TABLE I. For each inner sphere rotation rate f, we list the corresponding Rm, the total number Np of free parameters we invert for, the total number Nd of data points including mean measurements and time-varying magnetic data, and the associated global normalized misfit χ (the error-weighted rms difference between observations and predictions). The number of data points is much smaller at high Rm as ultrasound Doppler velocimetry is not operational. Values in parentheses are the numbers obtained when we do not invert for α and β.

f(Hz)	Rm	Np	Nd	χ
−9	28	108(96)	1130	1.5(1.8)
−15	47	108(96)	440	2.5(3.3)
−23	72	60(48)	230	2.5(4.9)
−30	94	60(48)	230	2.9(5.9)

to $l_{max} = 8$ ($m = 0$) and in Chebyshev polynomials in radius up to $n_{max} = 11$. $\alpha(r)$ and $\beta(r)$ are projected on Chebyshev polynomials up to $k_{max} = 5$, leading to

$$\mathcal{E}(r) = \sum_{k=0}^{5} T_k(r)(\alpha_k \langle \mathbf{B} \rangle + \beta_k \nabla \times \langle \mathbf{B} \rangle), \qquad (2)$$

where T_k is the degree k Chebyshev polynomial of the first kind and $\langle \mathbf{B} \rangle$ is the total mean magnetic field, solution of Eq. (1). Since the inversion is slightly nonlinear, we use the linearized least-squares Bayesian method of Tarantola and Valette [14], taking the *a posteriori* velocity model from a lower Rm, upscaled to the new Rm, as the *a priori* velocity model. We choose a zero value as the *a priori* model for all α_k and β_k. The poloidal velocity field is at least 1 order of magnitude smaller than the toroidal one. We do not invert for it at Rm = 72 and 94 but we include in the direct model a meridional flow upscaled from the solution obtained at Rm = 47 [9]. We find that solving for the emf, which adds only 12 degrees of freedom, reduces the global normalized misfit significantly (see Table I).

Figure 2 shows the radial profiles of α and β (with their *a posteriori* model errors) produced by the inversion of data

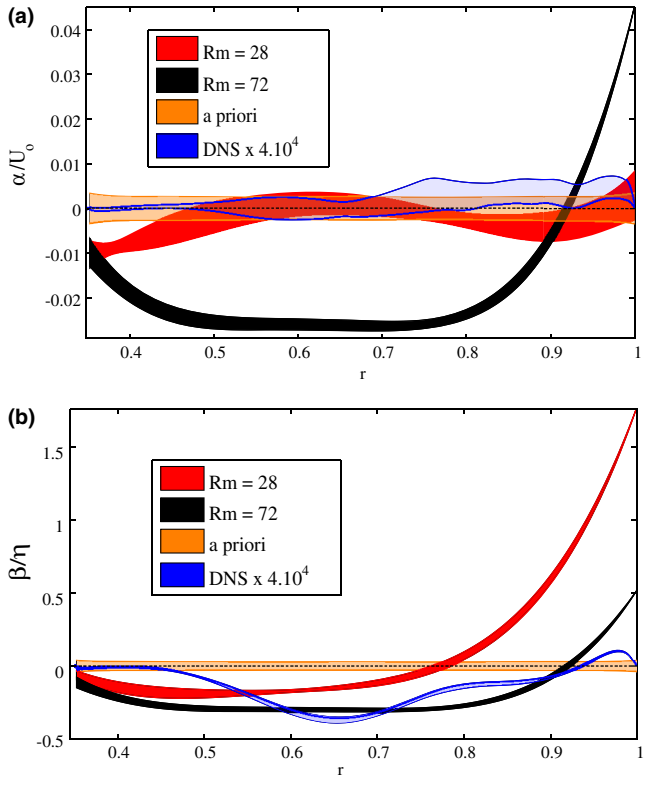

FIG. 2 (color online). Radial profiles of the α effect (a) and β effect (b) with their error bars, obtained by the inversion of DTS data for two magnetic Reynolds numbers: Rm = 28 and 72. The *a priori* null profile, along with its error bar, is also drawn. The blue curve shows the $\alpha(r)$ and $\beta(r)$ profiles retrieved from a numerical simulation of the DTS experiment at Rm = 29 and Re = 2.9×10^4, blown up by a factor 4×10^4.

at Rm = 28 and 72. The profiles for Rm = 94 (not shown) are almost the same as for Rm = 72. α is normalized by $U_0 = 2\pi f r_o$, and β by η. For the lower Rm value, we observe practically no α effect, while the $\beta(r)$ profile indicates that the β effect increases strongly when going from the Lorentz-force-dominated inner region to the Coriolis-force-dominated outer region. It reaches values of 1.7η near the outer boundary, where velocity fluctuations are strongest [12]. For the higher Rm, some α effect is required to match the data over most of the fluid domain. The $\beta(r)$ profile displays strongly negative values (down to -0.3η) over almost the complete fluid shell, but rises sharply to positive values near the outer boundary.

The introduction of the α and β effects clearly improves the fit to the measurements. We illustrate this in Fig. 3, which compares the prediction of our model, with and without the α and β terms, to the measurements of the time-varying signals for $f = -23$ Hz (Rm = 72), at a given latitude (−20°). There, a sleeve intrudes the sodium volume and records the azimuthal component of the magnetic field at six different radii labeled $P1$ to $P6$ (as drawn in Fig. 1). When the inner sphere spins, small deviations of its magnetic field from axisymmetry produce a magnetic signal that oscillates at the rotation frequency f and its overtones. Here, we focus on the $2f$ and $3f$ overtones caused by the $m = 2$ and $m = 3$ heterogeneities of the magnet. We measure the phase and amplitude of the time-varying magnetic signals at all six radii and plot them (with their error bars) in the complex plane, normalized by B_0 (the intensity of the imposed magnetic field at the equator of the outer shell). When the inner sphere is at rest, we record only the magnet's potential field weakening with increasing distance. Advection and diffusion completely distort this pattern when the inner sphere spins. The blue solid line displays the prediction from our full model of these magnetic signals from the largest values at the inner sphere boundary ($r = r_i$) to small values at the outer sphere ($r = r_o$). Symbols mark the radial positions of the $P6$ to $P1$

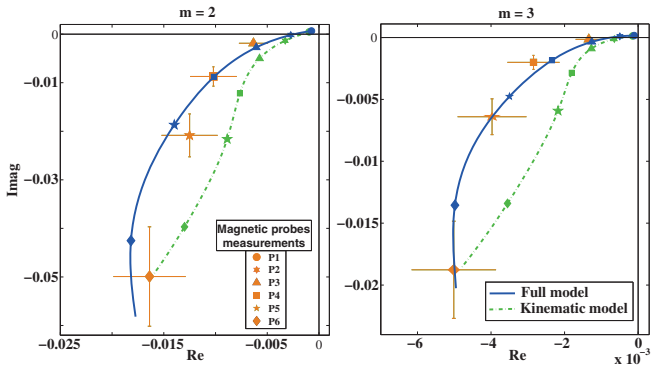

FIG. 3 (color online). Measurements and model fits for an example of time-varying magnetic signals measured at $2f$ ($m = 2$) and $3f$ ($m = 3$) frequencies, for a rotation rate of the inner sphere $f = -23$ Hz (Rm = 72). See the text for explanations.

magnetometers. The green dashed line is the trajectory predicted by our model when we remove the α and β terms. This altered model fails to produce the observations, indicating that the β effect that we retrieve contributes significantly to the measured signals.

In addition to the inversion of experimental measurements, we perform direct numerical simulations (DNS) of the experiment. Our code, based on spherical harmonic expansion [15] and finite differences in radius, has already been used to simulate the experiment. We restarted the most turbulent computation of Figueroa *et al.* [12] with a new imposed magnetic field containing the additional non-axisymmetric and nondipolar terms. This simulation reaches $\mathrm{Re} = 2\pi f r_o^2/\nu = 2.9 \times 10^4$ (ν is the kinematic viscosity), $\mathrm{Rm} = 29$, and a magnetostrophic regime close to that of the experiment [8]. Turbulence is generated by the destabilization of the outer boundary layer, yielding plumes that penetrate inward to regions of stronger magnetic fields. There, the velocity fluctuations are damped, but the associated magnetic fluctuations are stronger [12]. Six snapshots of the fields are saved every five turns. After we have reached a statistically steady regime, we average the fields over 162 turns of the inner sphere to obtain $\langle \mathbf{B} \rangle$ and $\langle \mathbf{U} \rangle$. It is then straightforward to compute the mean emf $\mathcal{E} = \langle \tilde{\mathbf{u}} \times \tilde{\mathbf{b}} \rangle$, where fluctuating fields are obtained from the difference between a snapshot and the time- and longitude-averaged field.

Meridional maps of the mean emf $\mathcal{E}_t$ are obtained and the latitudinal component is displayed in Fig. 4(a). The α and β profiles that best explain this mean emf (least-squares solution of Eq. (2) excluding high latitudes) are shown in Fig. 2. We estimate the error bar on the profiles as the standard deviation of emfs computed from five subsamples of 40 snapshots. One component of the emf $\mathcal{E}_{\alpha\beta}$ computed with these α and β profiles is shown in Fig. 4(b), and can be compared to the actual emf $\mathcal{E}_t$ [Fig. 4(a)]. Although the α and β profiles do not explain all of the mean emf, most features are recovered. Other components exhibit a similar behavior (not shown).

The parity (symmetry with respect to the equatorial plane) of the emf and of $\langle \mathbf{J} \rangle$ are clearly even [Fig. 4(c)], while $\langle \mathbf{B} \rangle$ is odd. This is in line with the fact that the DNS, just like the experiments at the lowest Rm, predicts no α effect [see Fig. 2(a)]. This might seem surprising given that the mean flow displays helicity. However, if we split the velocity fluctuations into even ($\tilde{\mathbf{u}}^+$) and odd ($\tilde{\mathbf{u}}^-$) parity, we see that their interaction with the mean odd magnetic field generates odd ($\tilde{\mathbf{b}}^-$) and even ($\tilde{\mathbf{b}}^+$) magnetic fluctuations, respectively. The resulting emf $\mathcal{E} = \tilde{\mathbf{u}} \times \tilde{\mathbf{b}}$ is therefore always even, if the odd and even velocity fluctuations are uncorrelated. This is likely true in the low Rm regime. The fact that the higher Rm-experiments require a nonzero α effect [Fig. 2(a)] reveals that the velocity fluctuations are interacting with an already-distorted larger-scale magnetic field, or that correlations between the two parities become nonzero.

The dipolar component of the induced magnetic field predicted by our full model is small but nonzero at the surface of the outer shell, even when the α effect is negligible. Spence *et al.* [3] have shown that an axisymmetric flow interacting with an axisymmetric magnetic field cannot produce an external dipole. This remains true if fluctuations only result in a homogeneous β effect. Even with a radially varying β effect as we obtain here, an external dipole can be produced only if a meridional flow is present.

The most striking feature of the $\beta(r)$ profiles we retrieve is the strong negative values (down to -0.3η) that span a large portion of the liquid sodium shell, especially at large Rm (see Fig. 2). The DNS supports this result, showing that

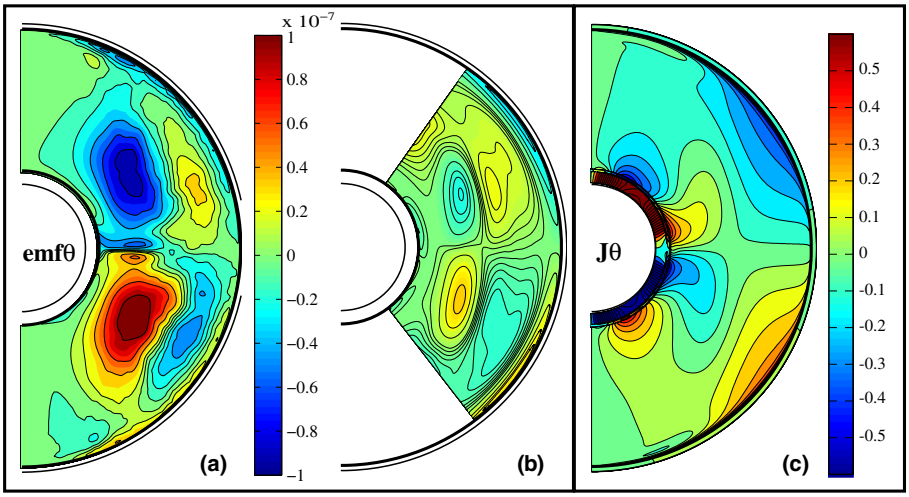

FIG. 4 (color online). Meridional cross section contour maps showing orthoradial component θ of emf $\mathcal{E}$ and of electrical current $\langle \mathbf{J} \rangle$. (a) Averaged emf $\mathcal{E}_t$ obtained from DNS. (b) Reconstructed emf $\mathcal{E}_{\alpha\beta}$ from inverted α and β profiles. High latitudes (white area) are excluded from the least-squares fit. (c) Mean electrical current from DNS.

it is not an artefact of considering only a radial dependence for α and β. The much lower amplitude of β in the DNS is due to a Reynolds number 300 times smaller than that in the experiment, suggesting that β may scale with Re^2. Although negative β values, and hence reduced magnetic diffusivity, are not unexpected [16–18], it is the first time that they are observed in experiment. Our DTS experiment combines a strong imposed magnetic field and strong rotation. These could be the ingredients that lead to this behavior. Were β to become even more negative, it might promote dynamo action.

This work was supported by the National Program of Planetology of CNRS-INSU under Contract No. AO2013-799128, and by the University of Grenoble. Most computations were performed on the Froggy platform of CIMENT [19], supported by the Rhône-Alpes region (CPER07_13 CIRA), OSUG@2020 LabEx (ANR10 LABX56), and Equip@Meso (ANR10 EQPX-29-01). We thank two anonymous referees and Elliot Kaplan for useful suggestions.

*henri-claude.nataf@ujf-grenoble.fr

[1] A. Gailitis, O. Lielausis, E. Platacis, S. Dement'ev, A. Cifersons, G. Gerbeth, T. Gundrum, F. Stefani, M. Christen, and G. Will, Phys. Rev. Lett. **86**, 3024 (2001).
[2] R. Stieglitz and U. Müller, Phys. Fluids **13**, 561 (2001).
[3] E. J. Spence, M. D. Nornberg, C. M. Jacobson, R. D. Kendrick, and C. B. Forest, Phys. Rev. Lett. **96**, 055002 (2006).
[4] P. Frick, V. Noskov, S. Denisov, and R. Stepanov, Phys. Rev. Lett. **105**, 184502 (2010).
[5] E. J. Kaplan, M. M. Clark, M. D. Nornberg, K. Rahbarnia, A. M. Rasmus, N. Z. Taylor, C. B. Forest, and E. J. Spence, Phys. Rev. Lett. **106**, 254502 (2011).
[6] K. Rahbarnia, B. P. Brown, M. M. Clark, E. J. Kaplan, M. D. Nornberg, A. M. Rasmus, N. Zane Taylor, C. B. Forest, F. Jenko, A. Limone, J.-F. Pinton, N. Plihon, and G. Verhille, Astrophys. J. **759**, 80 (2012).
[7] F. Ravelet, B. Dubrulle, F. Daviaud, and P.-A. Ratie, Phys. Rev. Lett. **109**, 024503 (2012).
[8] D. Brito, T. Alboussiere, P. Cardin, N. Gagnière, D. Jault, P. La Rizza, J.-P. Masson, H.-C. Nataf, and D. Schmitt, Phys. Rev. E **83**, 066310 (2011).
[9] S. Cabanes, N. Schaeffer, and H.-C. Nataf, arXiv:1407.2703.
[10] H.-C. Nataf, C.R. Phys. **14**, 248 (2013).
[11] V. Ferraro, Mon. Not. R. Astron. Soc. **97**, 458 (1937).
[12] A. Figueroa, N. Schaeffer, H.-C. Nataf, and D. Schmitt, J. Fluid Mech. **716**, 445 (2013).
[13] S. M. Tobias and F. Cattaneo, J. Fluid Mech. **717**, 347 (2013).
[14] A. Tarantola and B. Valette, Rev. Geophys. **20**, 219 (1982).
[15] N. Schaeffer, Geochem., Geophys., Geosys. **14**, 751 (2013).
[16] V. Zheligovsky and O. M. Podvigina, arXiv:physics/0207112.
[17] A. Brandenburg, K.-H. Rädler, and M. Schrinner, Astron. Astrophys. **482**, 739 (2008).
[18] A. Giesecke, F. Stefani, and G. Gerbeth, New J. Phys. **16**, 073034 (2014).
[19] https://ciment.ujf-grenoble.fr.